Tuning the interaction forces in tapping mode atomic force microscopy

Robert W. Stark,* Georg Schitter, and Andreas Stemmer
Nanotechnology Group, Swiss Federal Institute of Technology, ETH Center/CLA, CH-8092 Zurich, Switzerland
(Received 21 March 2003; published 7 August 2003)

The driving frequency is a key parameter to determine the tip-sample interaction forces in tapping mode atomic force microscopy (AFM). By adjusting the driving frequency slightly above the resonance frequency stable imaging with net attractive forces can be achieved almost independently from the quality factor of the cantilever. A reduction of the driving frequency below the resonance leads to a repulsive imaging regime with minimized repulsive forces. Numerical simulations as well as experiments show the influence on the interaction forces between tip and sample. Appropriate adjustment of the excitation frequency in dynamic AFM allows one to adjust the interaction forces over the entire range from net attractive to net repulsive.

DOI: 10.1103/PhysRevB.68.085401 PACS number(s): 68.37.Ps, 07.79.Lh, 07.05.Tp

I. INTRODUCTION

Dynamic atomic force microscopy (AFM) is a standard tool for the investigation of surface properties with nanometer resolution. In tapping mode (TM) AFM, highly resolved imaging of proteins is possible.[1–3] Depending on the oscillatory state of the system the forces between tip and sample may vary substantially. In the so-called ''low-amplitude'' or ''dominant attractive state'' high-resolution imaging of delicate samples is possible, whereas doing so in the ''high-amplitude'' or ''dominant repulsive state'' can lead to the destruction of the sample.[3,4] Thus, controlling the tip sample forces is a major prerequisite for high-resolution TM-AFM imaging in biological applications.

In TM-AFM the oscillation of the cantilever is restricted by the sample surface, which can be considered as a repulsive barrier defined by the elastic properties of the sample.[5–7] This interaction between tip and sample gives rise to nonlinear dynamics. From numerical simulations the existence of different oscillatory states[8–10] was deduced. By introducing an additional feedback circuit to increase the effective quality factor of the vibrating cantilever (Q control) the AFM can be stabilized in the low-amplitude regime.[11,12]

Basically, the micromechanical AFM cantilever is a multiple-degrees-of-freedom (MDOF) system allowing for higher eigenmode excitation.[13,14] These higher-order signals provide direct access to the time-resolved measurement of tip-sample interaction forces.[15] By comparing a numerical MDOF simulation with a single-degree-of-freedom (SDOF) analysis it was shown that already the SDOF approximation well reproduces important aspects of the dynamic behavior of the MDOF system, like the existence of a high- and a low-amplitude state.[16]

In the following we focus on the role of the driving frequency as a key parameter to set the imaging state in TM-AFM in ambient conditions. The behavior of tapping mode AFM is investigated at different driving frequencies with numerical simulations. Experiments illustrate how the selection of the driving frequency influences the imaging regime.

II. MODELING

In the harmonic oscillator approximation, the equation of motion is given by $m(d^2/dt^2)x+c(d/dt)x+kx=F(x,t)$. The parameter m is the effective mass, k the spring constant, c the viscous damping — e.g., in the surrounding air — and x the tip deflection. The external force consisting of the driving force $F_{\mathrm{dr}}(t)$ and the tip-sample force $F_{\mathrm{ts}}(x)$ is given by $F(x,t)=F_{\mathrm{dr}}(t)+F_{\mathrm{ts}}(x)$. The equation of motion is normalized by division with m and introducing the dimensionless time $\tau=t\omega_0$. With the resonance frequency $\omega_0^2=k/m$ and the quality factor Q defined by $c/m=\omega_0/Q$ one obtains

$$\ddot{x}+\frac{1}{Q}\dot{x}+x=\frac{F(x,\tau)}{k}, \tag{1}$$

where the overdot denotes $d/d\tau$. The driving force is given by $F_{\mathrm{dr}}(\tau)=F_{\mathrm{dr}}^0\sin(\beta\tau)$, where $\beta=\omega/\omega_0$ is the normalized driving frequency. For systems without or with negligible energy dissipation in the tip-sample contact the tip-sample force can be calculated using a Derjaguin-Müller-Toporov[17] (DMT) model:

$$F_{\mathrm{ts}}(x)=\begin{cases}-\dfrac{HR}{6(x+x_{\mathrm{s}})^2}, & x+x_{\mathrm{s}}\geqslant a_0,\\[2ex] -\dfrac{HR}{6a_0^2}+\dfrac{4}{3}E^*\sqrt{R}(a_0-x-x_{\mathrm{s}})^{3/2}, & x+x_{\mathrm{s}}<a_0,\end{cases} \tag{2}$$

where H is the Hamaker constant, R the tip radius, and x_{s} the distance of the sample from the tip's restposition. The parameter a_0 is an interatomic distance introduced[10] to avoid numerical divergence of F_{ts}. The effective tip-sample stiffness is given by $E^*=[(1-\nu_{\mathrm{t}}^2)/E_{\mathrm{t}}+(1-\nu_{\mathrm{s}}^2)/E_{\mathrm{s}}]^{-1}$, where E_{t} and E_{s} are the respective elastic moduli and ν_{t} and ν_{s} the Poisson ratios of tip and sample. Typical parameters for a silicon cantilever were chosen: $k=7.5\ \mathrm{N\,m^{-1}}$, $R=20$ nm, $E_{\mathrm{t}}=129$ GPa, and $\nu_{\mathrm{t}}=0.28$. The quality factor was set to $Q=100$, resulting in a resonant frequency of the forced system of $\omega_D=\omega_0\sqrt{1-1/(2Q)^2}=0.999\,99\omega_0$. A fused silica SiO_2 sample with $E_{\mathrm{s}}=70$ GPa, $\nu_{\mathrm{s}}=0.17$, $a_0=0.166$ nm, and $H=6.4\times10^{-20}$ J was assumed. The amplitude and sample positions x_{s} were normalized to the free amplitude $A_0=20$ nm at resonance frequency. The simulations were performed in MATLAB.[25]

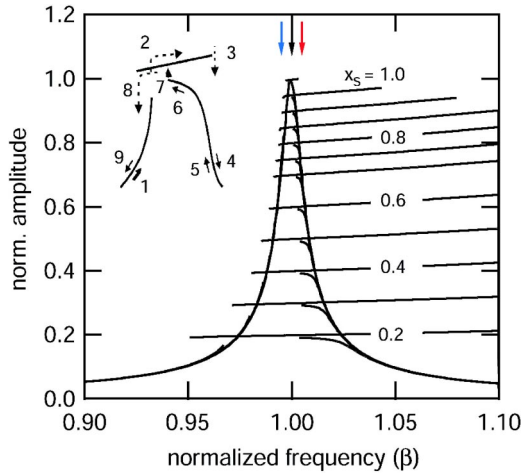

FIG. 1. (Color online) Amplitude response of the vibrating tip in response to a sweep cycle ($\beta=0.9\rightarrow\beta=1.1\rightarrow\beta=0.9$) simulated for different sample positions. Only physically accessible states are shown. The inset sketches the response of the system to a sweep cycle as indicated by the numbered arrows. The three arrows on top indicate where the approach retract cycles in Fig. 3 cut the resonance curve (sample positions $x_s=1.05$, 1.0, 0.95, 0.9, 0.85, 0.8, 0.75, 0.7, 0.6, 0.5, 0.4, 0.3, 0.2).

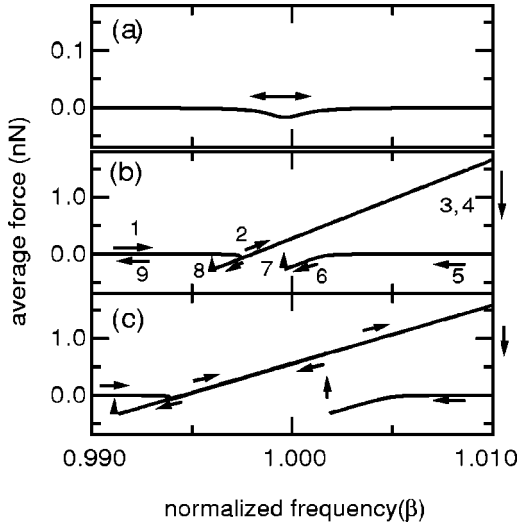

FIG. 2. Average interaction forces in a frequency sweep cycle at (a) $x_s=1.05$, (b) $x_s=0.95$, and (a) $x_s=0.75$. Note the small axis scaling in (a) as compared to (b) and (c).

Figure 1 shows the amplitude response of the vibrating tip at different sample positions x_s. The basic phenomena[18–20] are illustrated in the inset: Increasing the drive frequency the system response first is similar to that of an undisturbed harmonic oscillator (1). Then, increasing the frequency further also the amplitude response increases and the system is influenced by the surface potential. It transits to the plateau and follows it (2) until the system becomes unstable and transits back (3) to the behavior of an undisturbed oscillator (4). When the drive frequency is swept from high frequencies to low frequencies the system first follows the behavior of an undisturbed oscillator (5) until the surface forces influence the dynamic behavior. Attractive interaction forces induce a shift of the system resonance towards lower frequencies, leading to a neck in the resonance curve (6). Again, there is a transition to the plateau (7) followed by a transition (8) returning to the response of an undisturbed oscillator (9). From the numerical results shown in Fig. 1 it is evident that the plateau and depth of the neck depend on the sample position x_s.

The evolution of the average tip sample interaction forces $f_{\mathrm{avg}}=\int_0^{2\pi}F_{\mathrm{ts}}(\tau)d\tau$ during a frequency sweep cycle is shown in Fig. 2 for different sample positions x_s. In (a) at $x_s=1.05$ the tip remains in the attractive part of the interaction potential. Only weak attractive forces occur and no hysteresis is observed. Approaching the sample to $x_s=0.95$ the behavior changes as the tip enters the surface potential. From (b) it is evident that with the transition from the response of an undisturbed harmonic oscillator (1) to the plateau (2) also the interaction force changes. The interaction force almost linearly increases with increasing driving frequency until the state becomes unstable (3) and the system transits to the undisturbed oscillator (4) far away from the surface. Tuning the driving frequency downwards (5) reveals first a decrease in the average tip sample force (6) due to attractive interaction. This low-amplitude state becomes unstable and the system transits (7) to the high-amplitude solution. With decreased driving frequency the system follows the plateau to negative average interaction forces (8) until the system returns again to an undisturbed oscillation (9). Approaching the sample further this effect becomes more pronounced (c).

These plots show that the driving frequency is a key parameter for the operator to tune the tip-sample interaction forces. Experimentally, the driving frequency is usually set to the resonance frequency $\beta=1.000$. However, from Fig. 2 it is clear that there are other choices of a working frequency offering better imaging conditions. In order to image at small repulsive interaction forces the driving frequency should be reduced. For example at $x_s=0.75$ a reduction of the driving frequency from $\beta=1.000$ to $\beta=0.995$ reduces the average interaction force by an order of magnitude from $f_{\mathrm{avg}}=0.55$ nN to $f_{\mathrm{avg}}=0.04$ nN without changing the oscillatory state of the system (high-amplitude state) [Fig. 2(c)]. A further reduction of the driving frequency even leads to net attractive forces achieved with the high-amplitude state. Although the forces between tip and sample are small, the tip is in repulsive contact with the specimen. Repulsive imaging even at low forces is not favorable if chemical reactions or material transfer between tip and sample can occur, e.g., by physisorption or chemisorption of molecules from the specimen onto the tip.

If large forces are required, e.g., for surface modification by AFM lithography, the driving frequency can be adjusted accordingly. Large forces are achieved by first approaching the high-amplitude state and subsequently increasing the driving frequency. For imaging, a third option to adjust the interaction forces is most favorable. Setting $\beta=1.005$ and approaching carefully, the system can be kept in the low-amplitude state, leading to net attractive interaction forces. This is important if fragile samples like biomolecules are imaged by dynamic AFM.

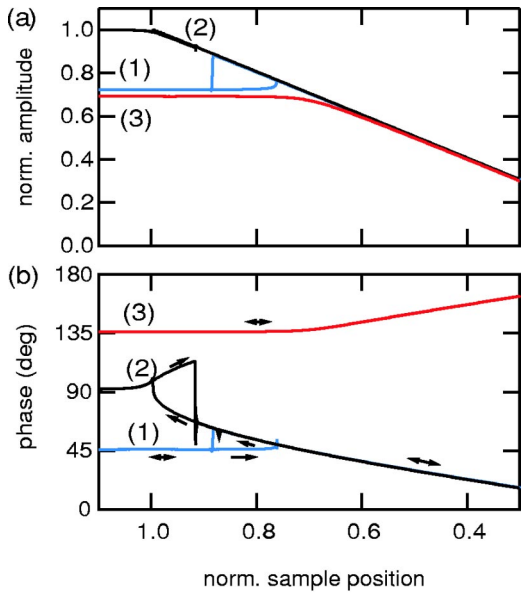

FIG. 3. (Color online) (a) Simulated amplitude and (b) phase in approach retract cycles at (1) $\beta=0.995$, (2) $\beta=1.000$, and (3) $\beta=1.005$. Curve (2) shows the typical hysteretic behavior with a transition from the low-amplitude state to the high-amplitude state. In contrast, with detuned driving frequencies the system only reaches the high-amplitude state or low-amplitude state, respectively.

Experimentally, dynamic approach and retract curves are valuable tools to characterize the tip-sample interaction. Performing force curves at different driving frequencies the amplitude response of the system can be investigated. This is illustrated by dynamic approach retract curves in Fig. 3 at the driving frequencies indicated by the three arrows on top of the resonance curve in Fig. 1. Choosing a driving frequency of $\beta=0.995$ the system is in the high-amplitude state [curve (1)]. At $\beta=1.000$ [curve (2)] the typical transition from the low-amplitude state to the high-amplitude state is observed. In contrast, in curve (3) at $\beta=1.005$ the system remains in the low-amplitude state without a transition to the high-amplitude state. Notably, this is achieved by selecting the appropriate driving frequency without manipulation of the quality factor.

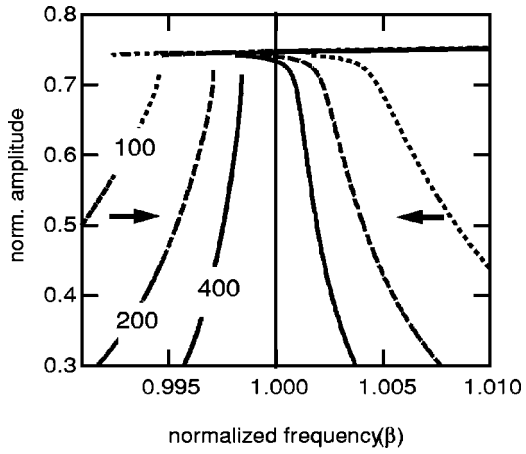

FIG. 4. Amplitude response to a frequency sweep simulated for different quality factors Q as indicated. The resonance peak of the system is narrowed with increasing Q factor and the neck is shifted towards lower frequencies ($x_s=0.75$).

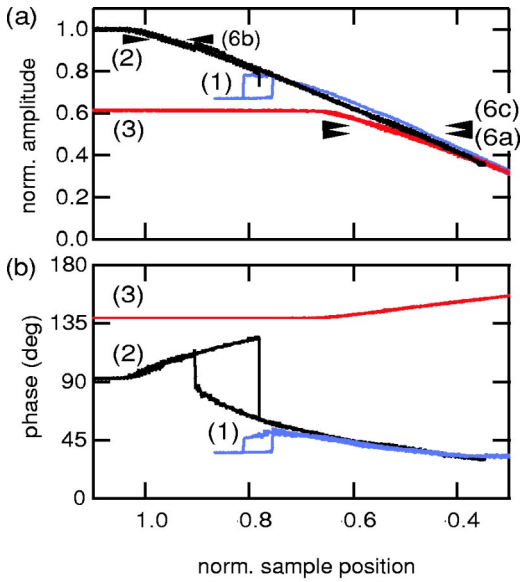

FIG. 5. (Color online) (a) Experimental amplitude and (b) phase in approach retract cycles at (1) $\beta=0.995$, (2) $\beta=1.000$, and (3) $\beta=1.006$. The curves well reproduce the behavior predicted in Fig. 3. The set points for the acquisition of the images in Figs. 6(a)–6(c) are indicated by the arrows.

Figure 4 shows the shape of the resonance curves for different quality factors. By increasing the quality factor the resonance curve becomes narrower and the neck shifts towards lower frequencies. It can be seen that with $Q=100$ there is no stable state for imaging in the small-amplitude solution—e.g., at $x_s=0.75$ and $\beta=1.000$. With increased Q net attractive imaging in the low-amplitude state becomes possible at $\beta=1.000$ as can be seen by the intersection of the line with the resonance curves. Thus, by selecting an appropriately high Q factor the imaging regime (high amplitude or low amplitude) can be set. But since the time constant for the decay of transients is proportional to Q, this is only achieved at the price of a significantly decreased scan velocity in amplitude detection feedback. From the discussion above it is clear that attractive imaging is possible even for cantilevers with lower Q factors at frequencies beyond the resonance frequency. Thus, for future high-speed atomic force microscopy[21–23] in tapping mode cantilevers with low Q factor should be selected because they allow one to achieve short response times together with attractive mode imaging.

III. EXPERIMENTAL RESULTS AND DISCUSSION

The experiments were carried out with a commercial atomic force microscope (MFP-3D, Asylum Research, Santa Barbara, CA, USA). For imaging and dynamic force spectroscopy, a silicon cantilever was used (experimental parameters $f_0=51.78$ kHz, $Q=134$; NSC 11, Lever A, MicroMasch, Tallinn, Estonia). The specimen, a cleaned object slide, was coated hydrophobically by 30 min immersion

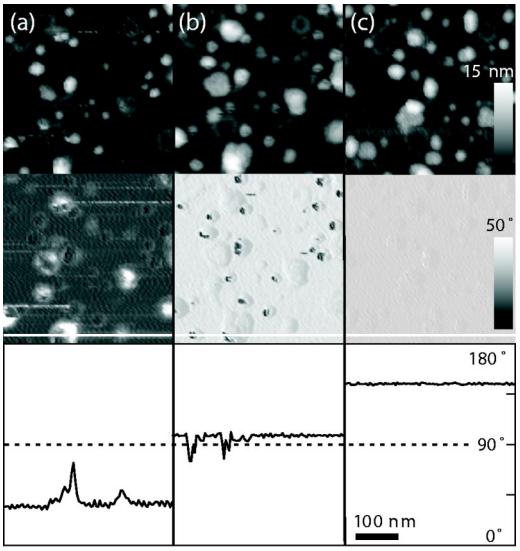

FIG. 6. Tapping mode AFM images of the silanized glass surface. The topography is shown in the top row, the phase lag in the middle and a cross sectional analysis of the phase in the bottom row. Data in column (a) were acquired at $\beta=0.995$, in (b) $\beta=1.000$, and in (c) $\beta=1.006$.

in a 2 mM solution of octadecyltrichlorosilane (OTS, Fluka) in toluene.

Figure 5 shows amplitude and phase during the approach and retract cycles on the silanized glass substrate. Curve (1) was measured at a driving frequency of $f_{(1)}=51.50$ kHz ($\beta=0.995$), curve (2) at $f_{(2)}=51.77$ kHz ($\beta=1.000$), and curve (3) at $f_{(3)}=52.10$ kHz ($\beta=1.006$). The curves reproduce the behavior predicted by our numerical simulations in Fig. 3 very well.

The images in Fig. 6 demonstrate the selection of the operating regime by adjusting the driving frequency. In the top row, topographic images of the silanized glass surface are shown. The grayscale (0–15 nm) and the image size (390 nm) are the same for all three images. The topographic images show a smooth surface together with polycondensated[24] OTS molecules. Apart from a first-order line-by-line leveling no data processing was performed. The respective phase images (raw data) are shown in the middle row. The grayscale spans 50° for all images; however, the offset was set individually to allow for optimal reproduction. The bottom row shows cross sections through the phase images as indicated by the white lines. The respective set point for the amplitude feedback of the AFM is indicated in Fig. 5.

The image in Fig. 6(a) was acquired in the high-amplitude state at a driving frequency below the resonance ($\beta=0.995$). The phase image reveals an average phase lag of $\phi_{\text{avg}}=35°$, and a contrast in the phase image indicates agglomerated silane molecules. This image contrast is due to variations in the local energy dissipation in the repulsive tip-sample interaction. Streaks in the image are due to external pertuberations or instabilities in the imaging process. At resonance frequency ($\beta=1.000$) the image was taken employing the low-amplitude state [Fig. 6(b)]. The average phase lag is $\phi_{\text{avg}}=96°$. However, there are instabilities (dark spots) in the phase image that indicate a transition to the high-amplitude state ($\phi=80°$). This bistable behavior is a consequence of the coexistence of high- and low-amplitude imaging states with comparable basins of attraction.[10] Increasing the set point to a larger amplitude led to unstable conditions, where the tip lost contact with the specimen, whereas a reduction of the set point resulted in increased fractions of the image being scanned in the high-amplitude state with $\phi=80°$ (data not shown). Thus, stable imaging employing the low-amplitude state could not be achieved by variation of the set point. By increasing the driving frequency ($\beta=1.006$) stable imaging in the low-amplitude state could be accomplished for more than 30 min. The phase image ($\phi_{\text{avg}}=146°$) demonstrates that transitions from the low-amplitude state to the high-amplitude state are absent.

IV. CONCLUSIONS

Theoretical considerations together with experiments show that the driving frequency is a key parameter to determine the tip-sample interaction forces in tapping mode atomic force microscopy. For tip-sample systems with negligible or small energy dissipation the average interaction forces can be tuned from net attractive over slightly repulsive to heavily repulsive simply by adjusting the driving frequency: At driving frequencies smaller than the resonance frequency small forces in the high-amplitude branch are obtained, whereas with driving frequencies slightly larger than the resonance frequency net attractive forces in the low-amplitude state are obtained without the need of an increased Q factor. This allows for stable imaging in the attractive regime.

*Electronic address: stark@nanomanipulation.de Current address: Section Crystallography, University of Munich, Theresienstr. 41, 80333 Munich, Germany.

[1] C. Möller, M. Allen, V. Elings, A. Engel, and D. Müller, Biophys. J. **77**, 1150 (1999).
[2] M. Stark, C. Möller, D. Müller, and R. Guckenberger, Biophys. J. **80**, 3009 (2001).
[3] A. San Paulo and R. García, Biophys. J. **78**, 1599 (2000).
[4] B. Pignataro, L. Chi, S. Gao, B. Anczykowski, C. Niemeyer, M. Adler, and H. Fuchs, Appl. Phys. A: Mater. Sci. Process. **74**, 447 (2002).
[5] N. Burnham, O. Behrend, F. Ouvelvey, G. Gremaud, P. Gallo, D. Gourdon, E. Dupas, A. Kulik, H. Pollock, and G. Briggs, Nanotechnology **8**, 67 (1997).
[6] O.P. Behrend, F. Oulevey, D. Gourdon, E. Dupas, A.J. Kulik, G. Gremaud, and N.A. Burnham, Appl. Phys. A: Mater. Sci. Process. **66**, 1 (1998).
[7] L. Nony, R. Boisgard, and J.P. Aimé, J. Chem. Phys. **111**, 1615 (1999).
[8] N. Sasaki, M. Tsukada, M. Tamura, R. Tamura, K. Abe, and N. Sato, Appl. Phys. A: Mater. Sci. Process. **66**, S287 (1998).
[9] M. Marth, D. Maier, J. Honerkamp, R. Brandsch, and G. Bar, J. Appl. Phys. **85**, 7030 (1999).
[10] R. García and A. San Paulo, Phys. Rev. B **61**, R13 381 (2000).

[11] B. Anczykowski, J.P. Cleveland, D. Krueger, V. Elings, and H. Fuchs, Appl. Phys. A: Mater. Sci. Process. **66**, S885 (1998).
[12] A.D.L. Humphris, A.N. Round, and M.J. Miles, Surf. Sci. **491**, 468 (2001).
[13] R.W. Stark and W.M. Heckl, Surf. Sci. **457**, 219 (2000).
[14] O. Sahin and A. Atalar, Appl. Phys. Lett. **79**, 4455 (2001).
[15] M. Stark, R.W. Stark, W.M. Heckl, and R. Guckenberger, Proc. Natl. Acad. Sci. U.S.A. **99**, 8473 (2002).
[16] T.R. Rodriguez and R. García, Appl. Phys. Lett. **80**, 1646 (2002).
[17] B.V. Derjaguin, V.M. Muller, and P. Toporov Yu, J. Colloid Interface Sci. **53**, 314 (1975).
[18] A. Kühle, A.H. Sørensen, and J. Bohr, J. Appl. Phys. **81**, 6562 (1997).
[19] L. Wang, Appl. Phys. Lett. **73**, 3781 (1998).
[20] A. San-Paulo and R. García, Phys. Rev. B **66**, 041406 (2002).
[21] M.B. Viani *et al.*, Rev. Sci. Instrum. **70**, 4300 (1999).
[22] G. Schitter, P. Menold, H.F. Knapp, F. Allgöwer, and A. Stemmer, Rev. Sci. Instrum. **72**, 3320 (2001).
[23] T. Sulchek, G. Yaralioglu, C. Quate, and S. Minne, Rev. Sci. Instrum. **73**, 2928 (2002).
[24] Y.A. Fadeev and T.J. McCarthy, Langmuir **16**, 7268 (2000).
[25] MATLAB, release 12, and SIMULINK, The MathWorks, Inc., Natick, MA. The simulations were integrated with ode23s, which is an implementation of an explicit Runge-Kutta (2,3) pair.